Computation of Convective Flow with Gravity Modulation in Rectangular Cavities

S. Biringen* and G. Danabasoglu†
University of Colorado, Boulder, Colorado 80309

In this work, a computational study is presented for the investigation of gravity modulation (g-jitter) effects in thermally driven cavity flows at terrestrial and microgravity environments. The two-dimensional, time-dependent Navier-Stokes equations are numerically integrated by a time-split method using direct matrix solvers. Computations at terrestrial gravity are utilized to assess the effects of adiabatic side-wall boundary conditions as well as the full nonlinearity of the governing equations on the sinusoidally forced Benard problem studied by Gresho and Sani.[1] The low-g calculations focus on the establishment of critical frequency ranges and consider the effects of modulation direction and randomness. The applicability of linear analysis in the excitable frequency range at low g is also discussed.

I. Introduction

THIS paper concerns a numerical study of two-dimensional cavity flows with gravity modulation emphasizing vibrational effects. In the space lab and Shuttle environments, the existence of perturbative accelerations, characterized by a broad frequency spectrum, is well known. These perturbations are caused by mechanical vibrations, Orbiter maneuvers, and crew activities and cannot be totally eliminated from the space manufacturing environment. An extensive overview of these and other sources of unsteady gravitational accelerations, derived from estimates based on measurements in the spacelab engineering model, has been documented elsewhere.[2] Accordingly, peak accelerations of 2.6×10^{-2} g due to crew activites are expected where g is terrestrial acceleration. Such undesirable perturbations during manufacturing processes affect heat and mass transfer and may have detrimental effects on the quality of material processed in space. This situation could be especially important in space-based crystal growth where the elimination/reduction of natural convection is essential to the quality of the crystals. The major goal of the present study is to obtain a fundamental understanding of some isolated aspects of fluid dynamic systems in an unsteady gravitational environment. Given that perturbative accelerations exist in the microgravity environment, we focus on estimating the critical frequency ranges that will drive a significant amount of convective motion, critical directions of modulation, and the effects of random forcing. It is anticipated that results of the type derived from this study will lead to a predictive modeling capability to assess the effects of gravity modulation (g-jitter) on fluid systems in a microgravity environment.

In addition to its relevance to microgravity, the effects of gravity modulation on Rayleigh-Benard convection is a problem of basic interest. Previous work by Gresho and Sani[1] considered this problem using the linearized equations of motion coupled with the nonlinear energy equation. With reference to a nonoscillatory system, they found that with heating from below, the flow is stabilized, but with heating from above, the flow can be destabilized. These results were confirmed by the recent three-dimensional, time-dependent numerical simulations of the full Navier-Stokes equations (Peltier and Biringen[3]). In another related work, Kamotani et al.[4] investigated the g-modulation problem at zero mean g in a two-dimensional square enclosure. Their mathematical model consists of the linearized equations for the fluctuating field and the steady-state equations for the mean field. They found that g modulation perpendicular to the direction of the temperature gradient is the most critical. In the present work, we investigate the effects of the full nonlinearity of the governing equations and establish some limits on the applicability of the linear models in the excitable frequency range. A summary of Russian work in this area primarily directed toward high-frequency vibration at zero mean-g level is also available in Ref. 5.

We consider a two-dimensional cavity with aspect ratio 2. Instead of the time-averaged, steady-state equations, the full Navier-Stokes equations are integrated through the transient phase. The effects of g-modulation direction and random oscillations representing more realistic conditions are also studied at one-g and low-g environments.

II. Governing Equations

In this section, we summarize the nondimensionalized equations of motion, energy, and continuity for an oscillating gravitational field along with the appropriate boundary conditions. These equations can be written as

$$\frac{\partial u}{\partial t}+\left(\frac{\partial u^2}{\partial x}+\frac{\partial uv}{\partial y}\right)=-\frac{\partial p}{\partial x}+Pr\left(\frac{\partial^2 u}{\partial x^2}+\frac{\partial^2 u}{\partial y^2}\right)+S_1 \quad (1)$$

$$\frac{\partial v}{\partial t}+\left(\frac{\partial uv}{\partial x}+\frac{\partial v^2}{\partial y}\right)=-\frac{\partial p}{\partial y}+Pr\left(\frac{\partial^2 v}{\partial x^2}+\frac{\partial^2 v}{\partial y^2}\right)+S_2 \quad (2)$$

$$\frac{\partial T}{\partial t}+\left(\frac{\partial Tu}{\partial x}+\frac{\partial Tv}{\partial y}\right)=\left(\frac{\partial^2 T}{\partial x^2}+\frac{\partial^2 T}{\partial y^2}\right) \quad (3)$$

$$\frac{\partial u}{\partial x}+\frac{\partial v}{\partial y}=0 \quad (4)$$

where

$$S_1=S_2=RaPrT\,[F_m+\eta\cos(\Omega t+\phi)] \quad (5)$$

Here, u and v are velocities along the x and y directions, respectively, and T, p, and t are temperature, pressure, and time, respectively. These equations represent two-dimen-

Presented as Paper 88-3727 at the 1st National Fluid Dynamics Congress, July 25-28, 1988, Cincinnati, OH; received June 21, 1989; revision received Sept. 11, 1989.

*Associate Professor, Department of Aerospace Engineering Sciences. Member AIAA.

†Graduate Student, Department of Aerospace Engineering Sciences.

sional, unsteady, laminar natural convection where the Boussinesq approximation is used for the buoyancy effect. Depending on the applied g-modulation direction, one of the source terms (either S_1 or S_2) is set equal to zero. In Eq. (5), F_m represents the constant (mean) gravity level such that $F_m = 1$ implies one g and $F_m = 0$ implies zero g. Also, η is the amplitude of the oscillatory part of the source term (corresponding to maximum modulation amplitude), and ϕ stands for random phase, which is set to zero for sinusoidal oscillation. Velocities are made nondimensional using the ratio of thermal diffusivity k to the cavity height h, whereas time and lengths are nondimensionalized by h^2/k and h, respectively. Finally, pressure is normalized by $\rho k^2/h^2$. Dimensionless temperature is defined by $(T-T_0)/(T_2-T_1)$ where T_1 and T_2 represent the cold and hot wall temperatures, respectively, and T_0 is the mean temperature in the cavity. Also, $Pr = \nu/k$ is the Prandtl number of the fluid, and Rayleigh number Ra is given as $Ra = [g\beta h^3(T_2-T_1)]/\nu k$, where g is the acceleration due to gravity, and β is the coefficient of thermal expansion. The nondimensional frequency is defined as $\omega = \Omega h^2/k$, where Ω is dimensional frequency, and the vibrational acceleration amplitude can be represented as $b\Omega^2/g$ modifying the definition of the Ra number at low gravity conditions.

The governing equations are solved subject to the following boundary conditions

$$y=0,\ 0\le x\le 1:\ u=v=0; \qquad T=0.5$$

$$y=1,\ 0\le x\le 1:\ u=v=0; \qquad T=-0.5$$

$$x=0 \text{ and } x=1,\ 0\le y\le 1:\ u=v=0; \qquad \partial T/\partial x=0 \qquad (6)$$

All of the calculations reported in this paper were started with zero velocity and temperature-initial fields.

III. Solution Method

The solution procedure consists of a semi-implicit approach using the explicit Adams-Bashforth method for the nonlinear convective terms and the implicit Crank-Nicolson method for the viscous terms. We implement the time-splitting method of Refs. 6-8, and the resulting decoupled momentum equations are solved on a staggered mesh using second-order central differences in space.

In the first step, the momentum equations are solved separately by a direct elimination procedure using L-U decomposition of the coefficient matrix. In the second step, an elliptic equation is solved for the pressure by the same direct elimination method satisfying continuity to machine accuracy. The same procedure was used for solving the energy equation. The direct solution of the five-point, finite-difference operator was accomplished using the International Mathematical and Statistical Libraries (IMSL) subroutines DLFTQS and DFLSQS, which take advantage of the sparseness and band-symmetry of these matrices. Note that all of the coefficient matrices are constant, and consequently the solution method necessitates L-U decomposition for each field variable only at the first time step. The factored matrices are stored and used for back substitution in the subsequent time steps providing significant economy in computational time. Typically, the code requires 0.61 s of CPU time per time step on a 41×21 grid on the VAX/VMS 8550 computer at the University of Colorado, Boulder. An extensive description of the method and results for test cases including shear and thermally driven cavity flows is given elsewhere.[8] The code was also successfully used to calculate oscillatory flow in low Pr fluids.[9]

IV. Results and Discussion

In this section, we present and discuss the results of the numerical simulations considering the effects of modulation direction, oscillation frequency, and amplitude at one-g and low-g environments (see Fig. 1). In the first part of this section, we provide a detailed comparison with the linear theory of Gresho and Sani[1] and present results from our nonlinear computations at terrestrial gravity (one g). The second part contains the nonlinear analysis of the zero-g cases.

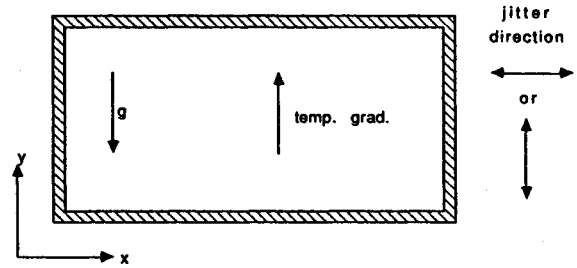

Fig. 1 Geometry of the cavity.

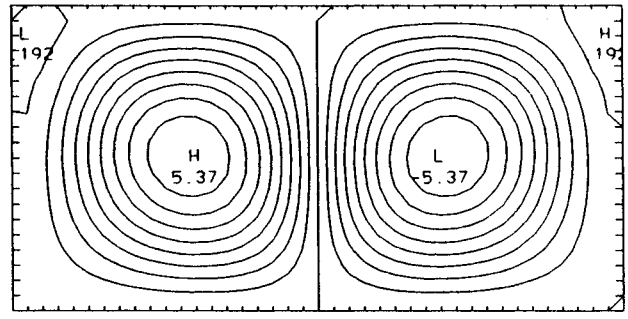

Fig. 2 Stream function [contour intervals (CI) = 0.6]: $Ra = 4500$, $Pr = 7$, one g ($\eta = 0$).

A. Numerical Simulations at Terrestrial Gravity

Computations at terrestrial gravity (one-g) conditions were primarily performed to investigate the effects of side walls on Benard convective with gravitational modulation. In these simulations, the Prandtl number was chosen as $Pr = 7$ in order to furnish a direct comparison with the results of Gresho and Sani[1] for infinite parallel plates, which they computed using the linearized equations of motion.

First, the results of $Ra = 4500$, $\eta = 0$ are obtained to serve as a reference; stream function, vorticity, and temperature contours for this case are given in Fig. 2. In this case, the temperature field was convective and the stream function contours (see Fig. 2) display two counter-rotating convection cells reflecting the characteristic pattern for a cavity with aspect ratio 2. The cells with negative contour levels rotate clockwise, those with positive contour levels rotate counterclockwise, and the selection mechanism for a particular rotation direction is likely a function of the initial conditions. Note that according to the stability diagram of Gresho and Sani,[1] the $Ra = 4500$ case is linearly unstable for a fluid layer heated from below. Accordingly, at this Rayleigh number, a modulation amplitude of $\eta = 19.6$ and modulation frequency of $\omega = 1400$ will stabilize this flow when gravity and temperature gradient are acting along the same direction. Here, $\eta = 19.6$ implies that the maximum amplitude of the oscillatory acceleration is 19.6 times terrestrial gravity. Although such high oscillatory amplitudes may not occur in practical situations, this case provides a direct comparison with Gresho and Sani.[1]

The results obtained by using these parameter values are displayed in Fig. 3. The time-averaged stream function contours indicate that the resulting flow is significantly modified in comparison with the $\eta = 0$ case. This is evidenced by weaker convection cells that have migrated toward the corners of the cavity; e.g., the maximum magnitude of the stream function is two orders of magnitude less than the previous case. In addition, the temperature field remained conductive due to the stabilizing influence of the modulation. This computation

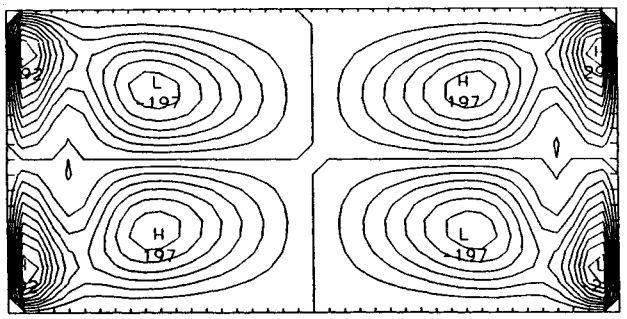

Fig. 3 Time-averaged stream-function contours ($CI = 0.3 \times 10^{-2}$) (in all of the velocity plots, A and B represent vertical and horizontal velocity components, respectively): $Ra = 4500$, $Pr = 7$, $\omega = 1400$, $\eta = 19.6$, one g (vertical).

demonstrates that adiabatic side-wall boundary conditions and the inclusion of the full nonlinearity of the governing equations do not affect the stabilizing influence of vertical g modulation using the parameters obtained from the linear analysis of Gresho and Sani.[1] In the subsequent calculation, we decreased η to 0.1 in order to isolate the effects of modulation amplitude. The resulting streamlines and isotherms were very similar to the $\eta = 0$ case indicating the existence of a critical value of η below which g modulation will not have a stabilizing influence.

Next, we consider the statically stable configuration of a cavity heated from the top. For this case, the parameters were chosen in accordance with Fig. 8 of Gresho and Sani,[1] i.e., $Ra = 14{,}985$, $\omega = 750$, and $\eta = 4.82$. These results are displayed in Figs. 6a-c in which time-averaged stream function contours depict the existence of three primary cells and two corner eddies; the corresponding temperature field is convective, demonstrating the destabilizing effect of this set of parameters. In addition to the contours of field variables, the time histories of u, v, and T were also recorded at several fixed locations in the cavity. These "points data" for the last two periods are shown in Fig. 4c and clearly show subharmonic response in complete agreement with Gresho and Sani.[1]

In their computational study of g modulation at zero gravity, Kamotani et al.[4] demonstrated that the most critical situation arises when the acceleration direction is perpendicular to the direction of the temperature gradient. In this section, this directional sensitivity of the flow is explored at terrestrial gravity. For this purpose, we performed a computation in which g modulation was applied horizontally, with $\omega = 1400$, $\eta = 19.6$, $Ra = 4500$, and $Pr = 7$. These results are illustrated in Fig. 5, and a comparison of Fig. 5a with Fig. 3a (corresponding to vertical g modulation with the same parameters) demonstrates the destabilizing effect of horizontal modulation when compared with vertical modulation. Accordingly, the variation of the modulation direction affects the cell structure transforming the eight-cell structure of Fig. 3a into one large primary cell and four small corner cells. An increase of several orders of magnitude in the stream function values is also indicated. Furthermore, the isotherms in Fig. 5b display a convective temperature field as opposed to the conductive isotherms in the vertical magnitudes (Fig. 5c) and temperature oscillations exhibit small deviations from a sinusoidal distribution, which may be caused by nonlinear interactions. Consequently, a given forcing function induces a faster flow if applied horizontally rather than vertically.

Using the same parameters, decreasing η from $\eta = 19.6$ to $\eta = 0.1$ indicated no significant change in the ensuing flowfield. In constrast, comparisons of this case with the corresponding vertical modulation with $\eta = 0.1$ demonstrated that even at these low amplitudes, directional variations affect the number of cells as well as the convective pattern of the isotherms.

In the following calculation, we considered the effects of randomizing the phase of the forcing function [designated ϕ in Eq. (5)] at each time step. The phase angle was normalized to vary between zero and 2π. The parameters used in this computation were $\omega = 1400$, $Ra = 4500$, $\eta = 19.6$, and $Pr = 7$, and g modulation was vertical. A comparison of the weakly convective flow resulting from this computation with the sinosoidally modulated case revealed that random forcing is only marginally more exciting than sinosoidal modulation with the same maximum amplitude.

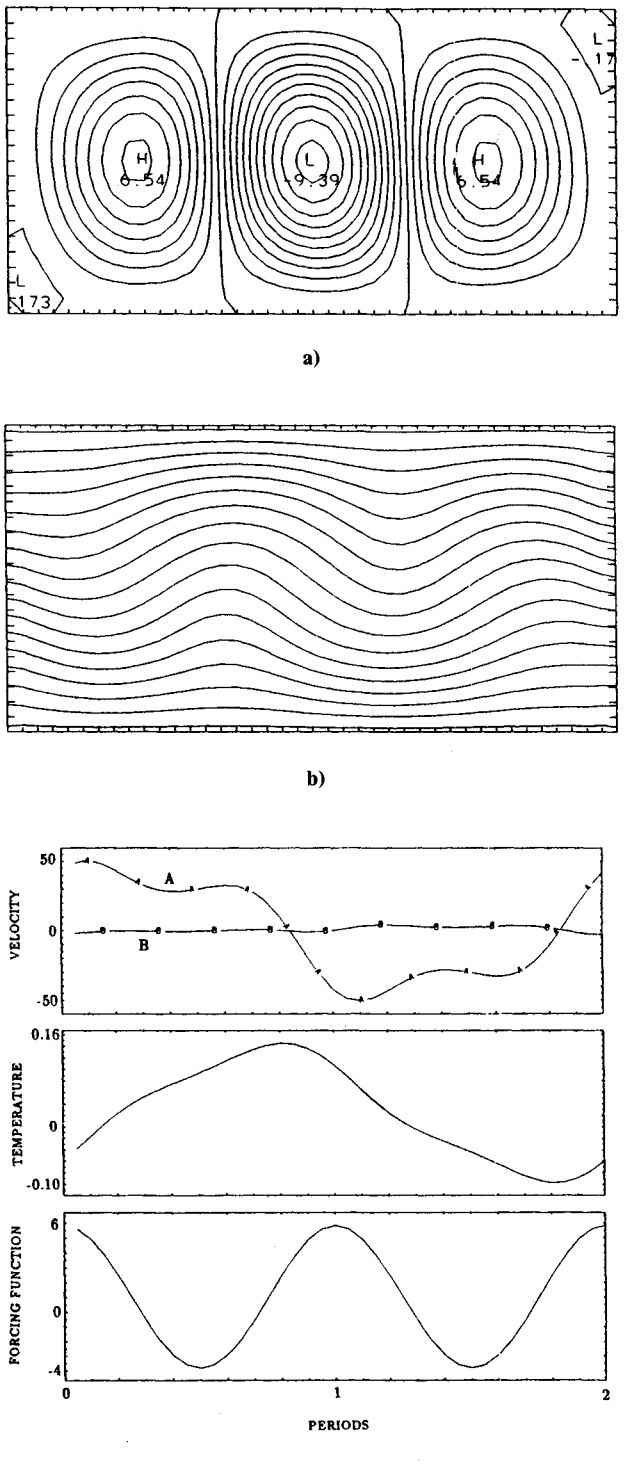

Fig. 4 a) Time-averaged stream-function ($CI = 0.9$) contours, b) time-averaged isotherms ($CI = 0.06$), and c) point data history; $Ra = -14{,}985$, $Pr = 7$, $\omega = 750$, $\eta = 4.82$, one g (vertical).

B. Numerical Simulations at Zero Gravity: Nonlinear Analysis

In this section, a parametric study of g modulation at zero-g environment is presented. In particular, attention is focused on the effects of modulation frequency and direction. Because the materials of interest for low-gravity applications typically have low Prandtl numbers, in these computations we set $Pr = 7 \times 10^{-3}$ corresponding to germanium. The viscosity and the coefficient of thermal expansion of this material are $1.54 \times 10^{-7} m^2/s$ and $10^{-4} K^{-1}$, respectively. In accordance with the spacelab experiments,[2] we assumed a peak vibrational acceleration level of $10^{-2} - 10^{-3}$ g, where g is the terrestrial gravitational acceleration. Using 100 K for the temperature gradient and $h = 18$ cm as the characteristic length of the cavity, a typical Rayleigh number $Ra = 1.771 \times 10^5$ based on maximum acceleration can be calculated. All of the numerical experiments discussed in this section were performed using this Rayleigh number. For low Pr numbers, the resolution requirements become more stringent in order to capture the hydrodynamic and thermal boundary layers. This is especially important for high Ra numbers at terrestrial gravity. In the present work, since the low Pr number cases were calculated at zero-base gravity, this requirement was met with the uniform 33×33 grid even at the exciting frequencies where velocity and temperature gradients are sharper.

In the first set of these computations, the cavity was subjected to vertical modulation along the direction of the tem-

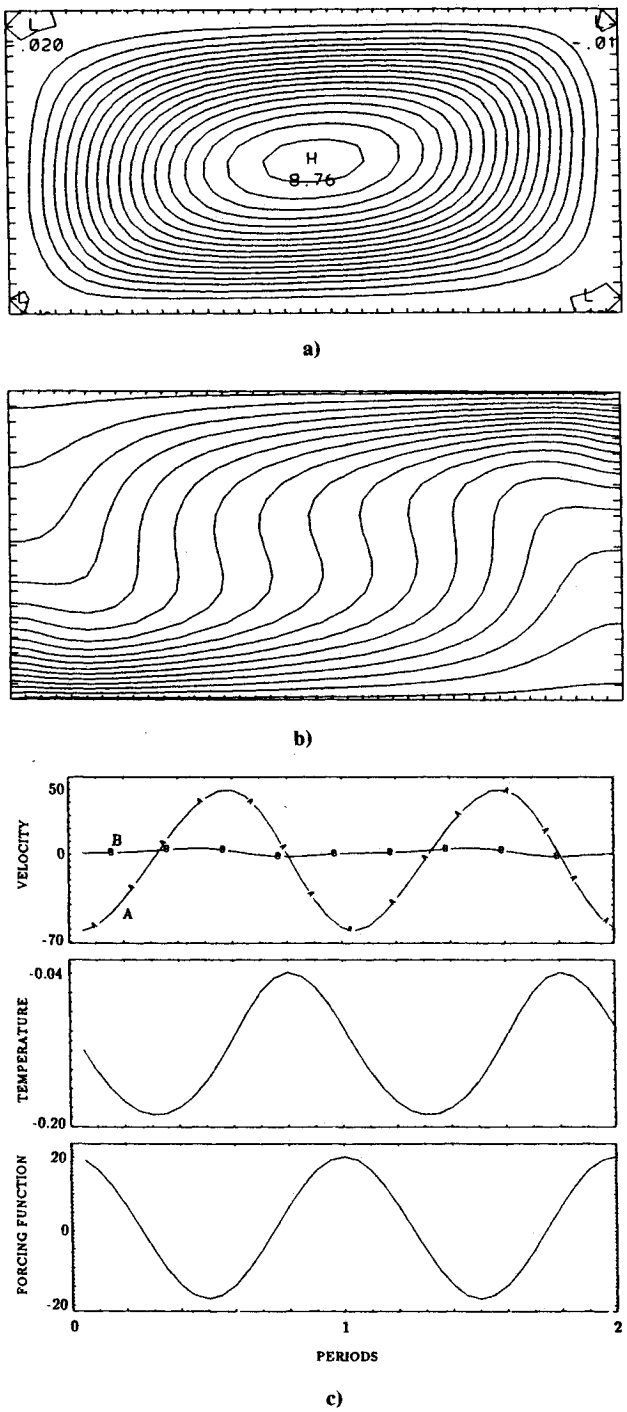

Fig. 5 a) Time-averaged stream-function ($CI = 0.5$) contours, b) time-averaged isotherms ($CI = 0.06$), and c) point data history; $Ra = 4500$, $Pr = 7$, $\omega = 1400$, $\eta = 19.6$, one g (horizontal).

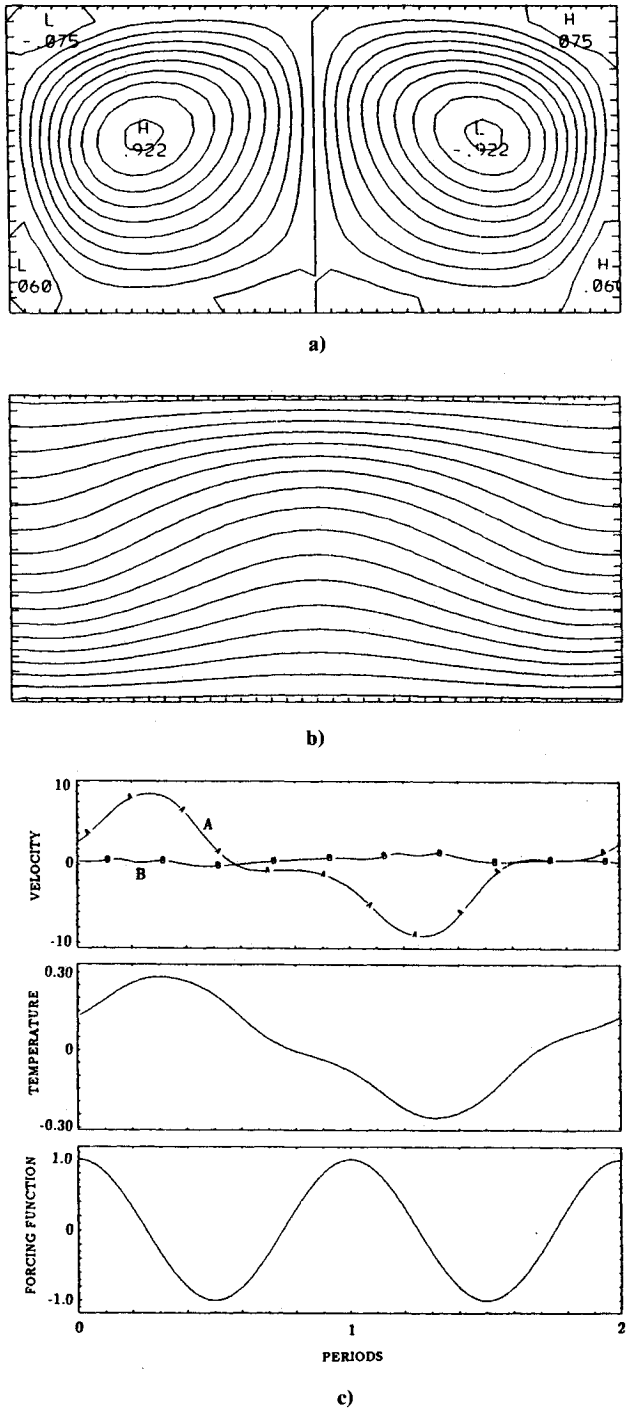

Fig. 6 a) Time-averaged stream-function ($CI = 0.1$) contours, b) time-averaged isotherms ($CI = 0.06$), and c) point data history; $Ra = 1.771 \times 10^5$, $Pr = 7 \times 10^{-3}$, $\omega = 20$, zero g (vertical).

Table 1 Maximum stream function values as a function of the nondimensional frequncy parameter ω for the time-averaged results (vertical)

ω	max $\lvert\psi\rvert$
4543	0.984×10^{-8}
45.5	0.335×10^{-2}
30	0.239×10^{-2}
20	0.922

perature gradient, and the critical range of exciting frequencies was explored starting with $\omega = 45.5$. Note that $\omega = 45.5$ can be interpreted as $\Omega = 4.92 \times 10^{-3}$ Hz for $h = 18$ cm or $\Omega = 17.7$ Hz for $h = 3$ mm. For this case, system response was synchronous with the forcing function, and the isotherms were conductive.

The effects of lower frequencies were probed by setting $\omega = 20$; the results of these computations are displayed in Figs. 6. In Fig. 6a, the time-averaged stream function contours indicate two counter-rotating cells accompanied by several secondary vortices. The stream function attains values several orders of magnitude higher than the previous cases, and the isotherms are convective (Fig. 6b). Point data illustrated in Fig. 6c indicate subharmonic response. Table 1 displays the maximum values of the stream function obtained in the cavity as a function of the nondimensional frequency. At the transition point from conductive to convective temperature field, there is a significant jump in the time-averaged values of the stream function.

The second set of numerical experiments at zero gravity were conducted with g modulation imposed along the direction perpendicular to the temperature gradient with $Ra = 1.771 \times 10^5$ and $Pr = 7 \times 10^{-3}$. Note that this configuration was found to be most critical at terrestrial gravity. As before, we started with a relatively high value of ω and searched for the destabilizing frequency range by systematically reducing the value of this parameter.

For this configuration, the onset of temperature excitation is observed when ω is set equal to 200 (Fig. 7). In Fig. 7a, the time-averaged stream function contours depict a tilted primary vortex, and two counterclockwise rotating eddies are formed at the corners of the cavity. The isotherms indicate the onset of convective excitation, which increases the maximum average Nusselt number (Fig. 7c). As in the previous cases, system response is synchronous with the forcing frequency. Here we define the Nusselt number

$$Nu = -\frac{\partial T}{\partial y} + uT \tag{7}$$

The next case corresponds to $\omega = 85$ and develops a strongly excited, convective flow as evident from the time-averaged stream function contours (Fig. 8a) and the Nusselt number distribution (Fig. 8c). At this frequency, small-scale eddies start to develop, and the temperature point data display deviations from periodicity (see Fig. 11), which are likely caused by strong nonlinear effects. As indicated in Fig. 8c, high temperature gradients instigated by this convective excitation lead to a significant increase in the time-averaged Nusselt number.

From the previous analyses, it is evident that because a range of resonant frequencies for the cavity flow is being approached, a further reduction of ω should be of interest. Consequently, in Figs. 9, we present the results for a case with $\omega = 50$, which corresponds to a dimensional frequency of 5.41×10^{-3} Hz for $h = 18$ cm. The time-averaged stream function plot (Fig. 9a) shows two irregular-shaped counter-rotating cells in the cavity. The point data (Fig. 9b) indicate strong deviations from sinusoidal response, which must be regarded as a consequence of the energy transfer to and the nonlinear coupling of higher modes. The distribution of the averaged Nusselt number (Fig. 9c) displays two local maxima with high magnitudes.

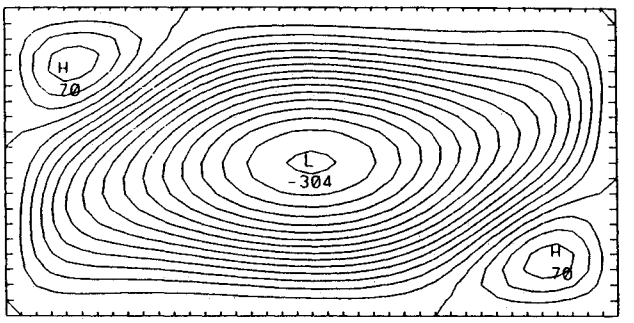

a)

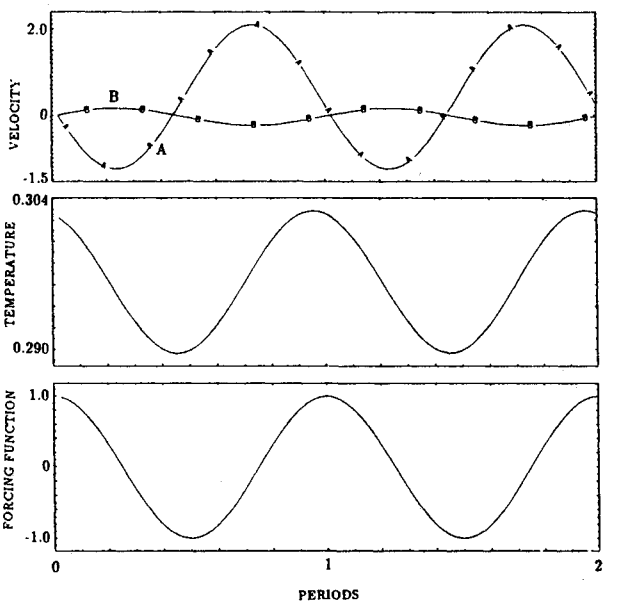

b)

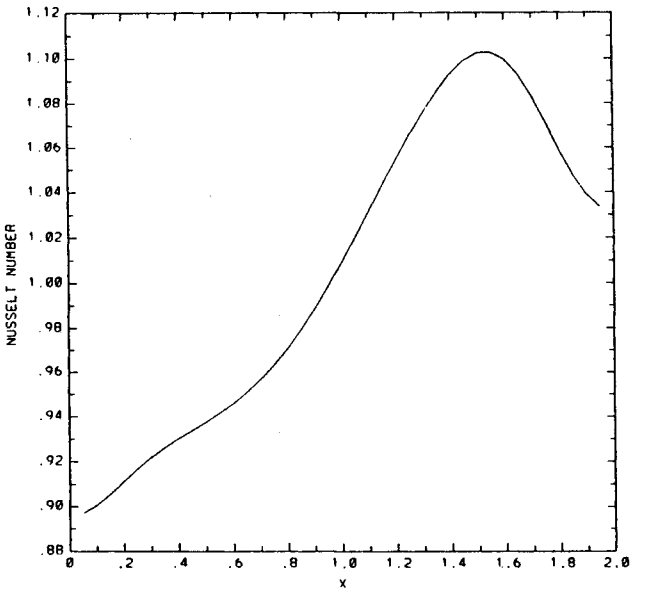

c)

Fig. 7 a) Time-averaged stream-function ($CI = 0.02$) contours, b) point data history, and c) time-averaged Nusselt number distribution on the heated wall: $Ra = 1.771 \times 10^5$, $Pr = 7 \times 10^{-3}$, $\omega = 200$, zero g (horizontal).

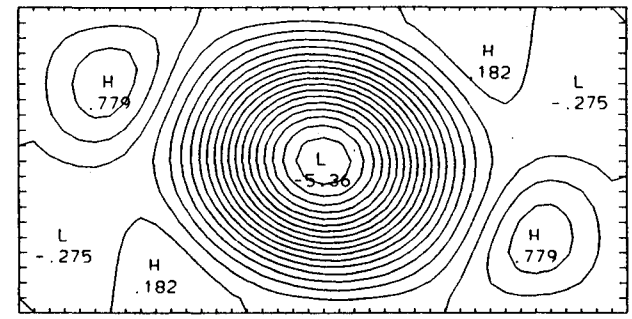

a)

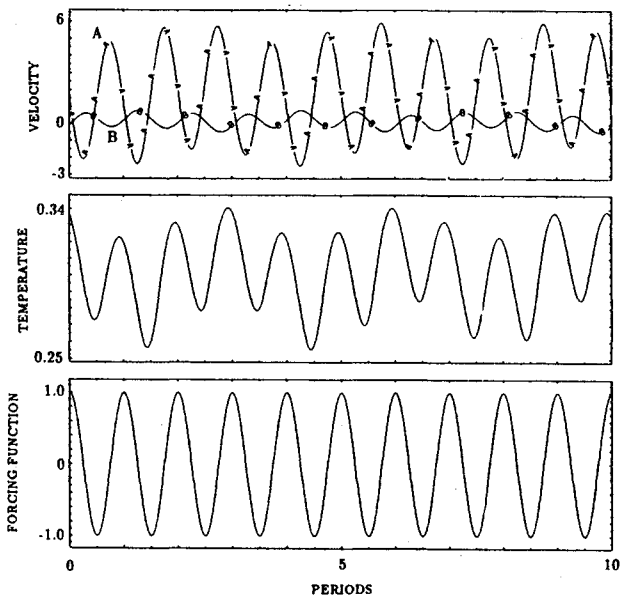

b)

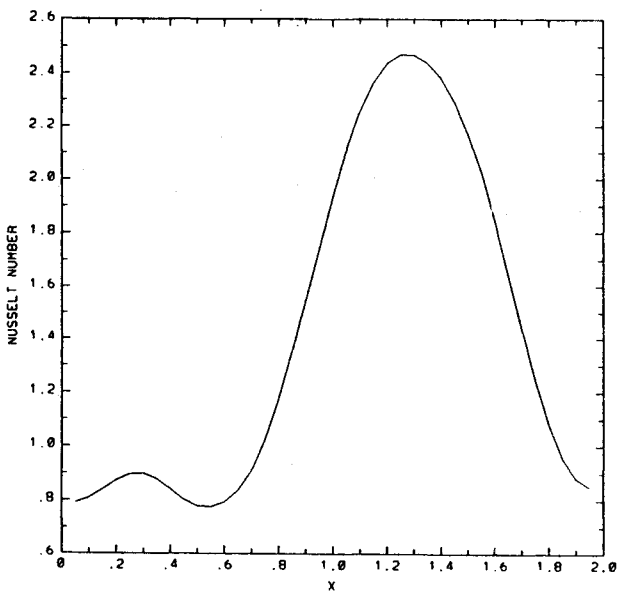

c)

Fig. 8 a) Time-averaged stream-function ($CI = 0.3$) contour, b) point data history, and c) time-averaged Nusselt number distribution on the heated wall: $Ra = 1.771 \times 10^5$, $Pr = 7 \times 10^{-3}$, $\omega = 85$, zero g (horizontal).

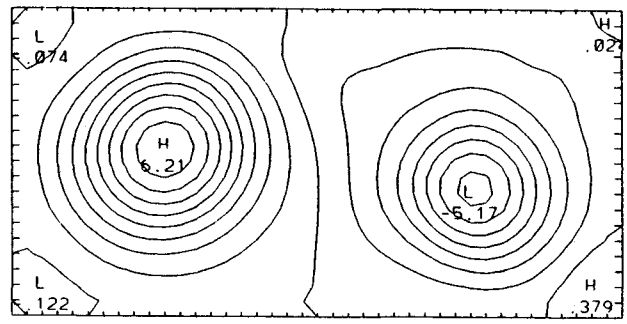

a)

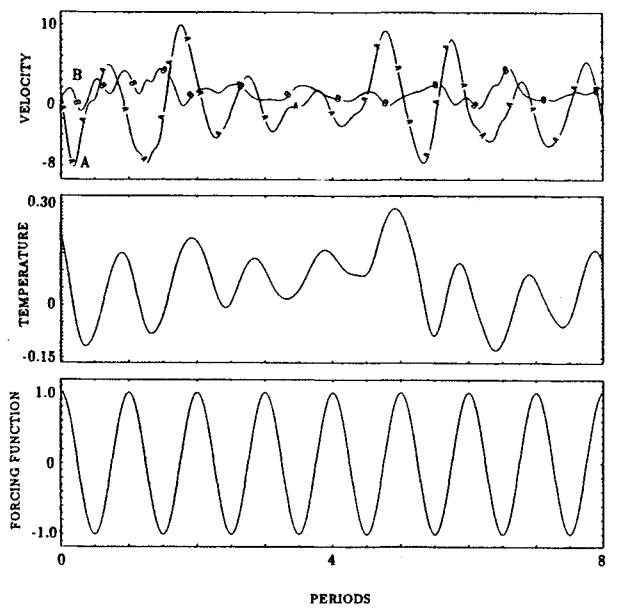

b)

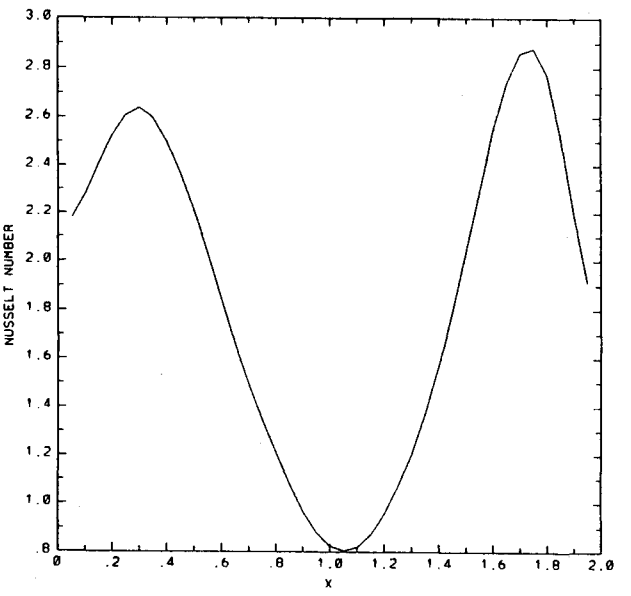

c)

Fig. 9 a) Time-averaged stream-function ($CI = 0.7$) contour, b) point data history on the horizontal centerline close to the cavity center, and c) time-averaged Nusselt number distribution on the heated wall: $Ra = 1.771 \times 10^5$, $Pr = 7 \times 10^{-3}$, $\omega = 50$, zero g (horizontal).

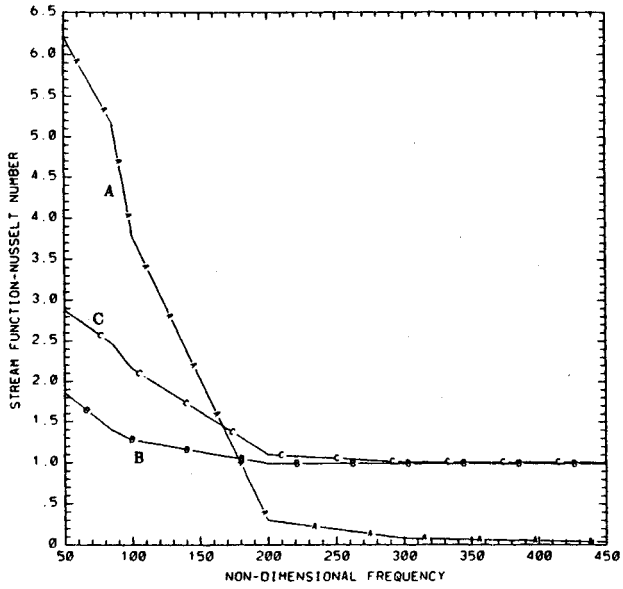

Fig. 10 The variations of the maximum value of the stream function (*A*) and the averaged (*B*) and maximum (*C*) values of Nusselt number as a function of the nondimensional frequency for the time-averaged, horizontal modulation cases.

In Fig. 10, the variation of the averaged (*B*) and maximum (*C*) values of Nusselt number and the maximum value of the stream function (*A*) are plotted as functions of ω for the horizontal modulation cases. It is observed that transition to convection occurs between $\omega = 250$ and $\omega = 200$, as evidenced by the signficant magnitude increase of all the variables plotted in this figure. Note also that for the cases with conduction isotherms, the average and the maximum Nusselt numbers remain very close to unity.

It is also of interest to investigate the response of the excited flows to the removal of the forcing function in order to provide an estimate for the characteristic time required for the convective flow to restore to its original quiescent state. This issue is of relevance to the space manufacturing environment where typically the forcing is an impulse function. For this purpose, we calculated a case in which the converged results of $\omega = 85$ (with horizontal modulation) were incorporated as the initial conditions and the modulation amplitude is set to zero. These results are included in Figs. 11a and 11b at the nondimensional time equal to 8.4, corresponding to 114 periods of the forcing function. This nondimensional time was equivalent to approximately 38 s with $h = 1$ cm and 0.38 s with $h = 1$ mm. System response is presented in Fig. 11b and reveals the attenuation of the velocity and temperature magnitudes at a fixed point in the cavity. As expected from the high heat diffusive nature of this low *Pr* material, temperature oscillations are damped much faster than the velocity oscillations. The corresponding stream function contours of the residual field (Fig. 11a) demonstrate that the maximum stream function magnitude is about 20 times less than its initial value. At this stage in the computation, the isotherms are already conductive.

Finally, we performed a numerical experiment to investigate the effects of increasing Prandtl number by setting $Pr = 0.71$. All of the other parameter values corresponded to the case with $Pr = 7 \times 10^{-3}$, $\omega = 85$, and horizontal modulation. These results are included in Figs. 12. A comparison of the time-averaged results displayed in Figs. 12a with the related low *Pr* case (Fig. 9a) indicates the effects of increasing the *Pr* number of the time-averaged flow. With increasing *Pr*, the maximum value of the stream function decreases, and the secondary corner eddies strengthen in contrast with the results of Kamotani et al.[4] Furthermore, as expected, the temperature field becomes more exciting in comparison with the low *Pr* case. The system response for the velocity components and the temperature at a fixed point in the cavity are presented in Fig. 12c. These data include the last four periods and display the strong nonlinearity of the flowfield. Here, both the vertical velocity component and temperature are nearly 180 deg out of phase with the forcing function. The average Nusselt number variations along the hot (bottom) wall are plotted in Fig. 12c for several instants in time. The time-averaged distribution remains symmetric and shows that increasing the Prandtl number results in higher heat transfer rates.

According to the results of Kamotani et al.,[4] the maximum value of the time-averaged stream function increases with increasing the *Pr*. However, as just discussed, our full Navier-Stokes simulations at the strongly exciting frequency of $\omega = 85$ indicate otherwise. In order to investigate the underlying cause of this difference, we performed two calculations with $Pr = 7 \times 10^{-3}$ and $Pr = 0.71$ shutting off the nonlinear terms in the momentum equations. The resulting time-averaged stream function contours are displayed in Figs. 13 and 14 and reveal the limits of the linear model as applied to the *g*-modulation problem. For $Pr = 0.71$, even after 210 oscillation periods, the resulting flow was quasisteady, i.e., the period-averaged stream function maximum values varied between about 6 and 22 and always remained higher than the lower *Pr* case. In Fig. 14, the period-averaged stream function contours are plotted

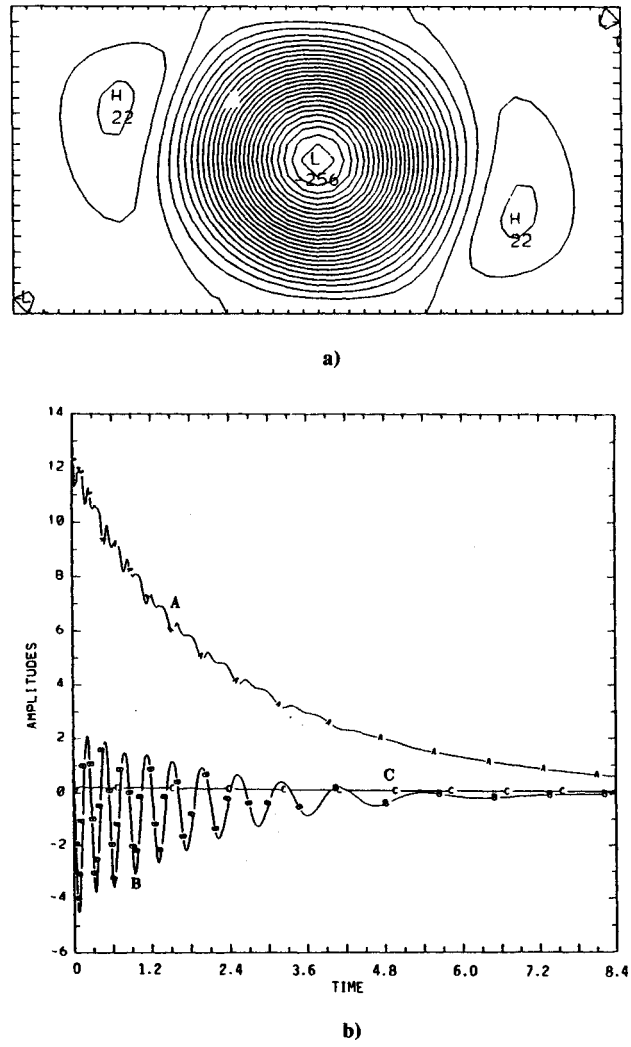

Fig. 11 a) Stream-function (*CI* = 0.01) contours at $t = 8.4$; and b) point data history at the horizontal centerline close to the cavity center, [vertical (*A*) and horizontal (*B*) velocity components and temperature (*C*)]: $Ra = 1.771 \times 10^5$, $Pr = 7 \times 10^{-3}$, zero *g* (no modulation).

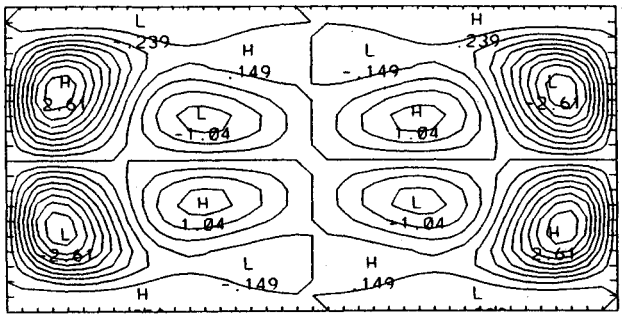

a)

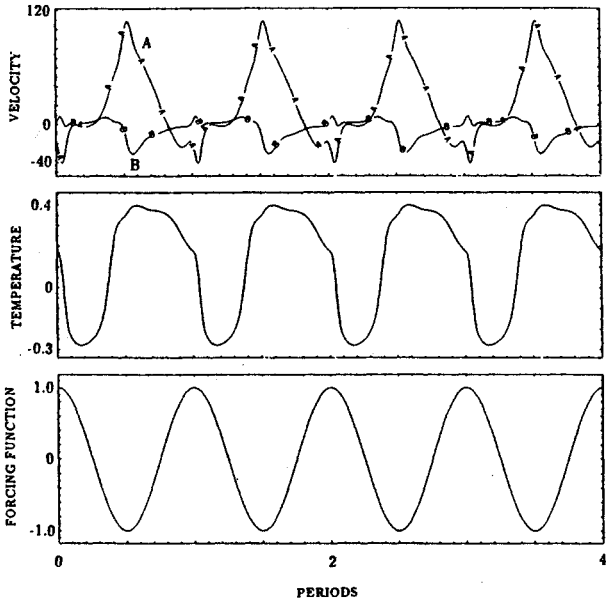

b)

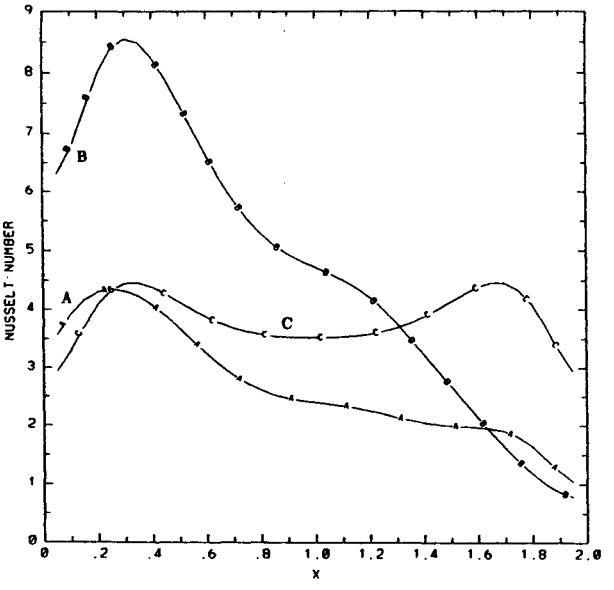

c)

Fig. 12 a) Time-averaged stream-function contours ($CI = 0.3$), b) point data history near the lower left corner, and c) Nusselt number distribution on the heated wall (A) at $t = 0$, (B) at $t = \pi/2$, (C) time-averaged: $Ra = 1.771 \times 10^5$, $Pr = 0.71$, $\omega = 85$, zero g (horizontal).

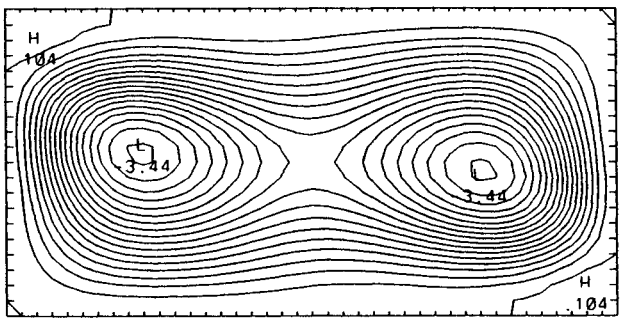

Fig. 13 Time-averaged stream-function ($CI = 0.2$) contours: $Ra = 1.771 \times 10^5$, $Pr = 7 \times 10^{-3}$, $\omega = 85$, zero g (horizontal).

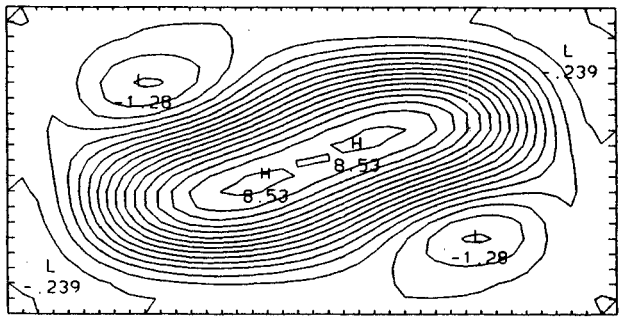

Fig. 14 Time-averaged stream-function ($CI = 0.6$) contours: $Ra = 1.771 \times 10^5$, $Pr = 0.71$, $\omega = 85$, zero g (horizontal).

at the 207th period. This increase with increasing Pr number is in accordance with Kamotani et al.[4] but is in contrast to our corresponding full Navier-Stokes simulations. Consequently, it is feasible to assert that the nonlinear terms should not be omitted for the cases with low, resonant frequencies that excite the flow since it may lead to a different flow than is predicted by the full equations. However, a comparison of the linear cases with the full simulations indicated that the temperature field is mildly affected and that the point data history is almost invariant.

V. Concluding Remarks

In this work we investigated the effects of gravity modulation on thermally driven, two-dimensional cavity flows with aspect ratio 2 at both terrestrial and microgravity environments. A parameteric study was performed to isolate the effects of nondimensional frequency as well as modulation amplitude and direction.

In accordance with Gresho and Sani,[1] our results show that it is possible to stabilize an otherwise unstable flow using certain frequency and amplitude parameter combinations at terrestrial gravity with vertical g modulation. Furthermore, a statically stable configuration can be excited in the same manner. Our results are in full agreement with the analysis of Gresho and Sani[1] confirming the accuracy of our numerical model and establishing that, for the Rayleigh numbers and the frequency ranges considered, side-wall boundary conditions and the inclusion of the nonlinear terms are not significant. As evidenced from our computations, g modulation perpendicular to the imposed temperature gradient is the most critical, whereas the effects of random forcing are marginal.

For low-g calculations with a low Prandtl number, the temperature field becomes more excitable with decreasing frequency for both horizontal and vertical modulation. It is also shown that horizontal modulation is more effective in instigating a transition from a conductive to a convective temperature field at higher frequencies. The removal of the forcing func-

tion shows that g-modulation effects can persist for a significant time. The persistance of the velocity oscillations and the recirculation cells, even when the thermal field is conductive, could be of importance in mass transport in the presence of impurities. Finally, we demonstrate that the inclusion of the nonlinear, convective terms in the momentum equations is necessary for the simulation of the g-modulation problem at zero g in the excitable frequency range with horizontal modulation.

Acknowledgments

This work was supported by NASA Grant NAGW-951 to the Center for Low Gravity Fluid Mechanics and Transport Phenomena, University of Colorado, Boulder. The authors thank Jean N. Roster for helpful discussions.

References

[1]Gresho, P. M., and Sani, R. L., "The Effects of Gravity Modulation on the Stability of a Heated Fluid Layer," *Journal of Fluid Mechanics*, Vol. 40, No. 4, 1970, p. 783-806.

[2]Knabe, W., and Eilers, D., "Low Gravity Environment in Spacelab," *Acta Astronautica*, Vol. 9, No. 4, 1982, p. 182-198.

[3]Biringen, S., and Peltier, L. J., "Numerical Simulation of 3-D Benard Convection with Gravitational Modulation," *Physics of Fluids A*, Vol. 2, No. 5, 1990, p. 754-764.

[4]Kamotani, Y., and Prasad, A., and Ostrach, S., "Thermal Convection in an Enclosure Due to Vibrations Aboard Spacecraft," *AIAA Journal*, Vol. 19, No. 4, 1981, p. 511-516.

[5]Gershuni, G. Z., and Zhukhovitskiy, Y. M., "Vibration-Induced Thermal Convection in Weightlessness," *Fluid Mechanics Soviet Research*, Vol. 15, No. 1, 1986, p. 63-84.

[6]Fortin, M., Peyret, R., and Temam, R., "Résolution Numérique des Équations de Navier-Stokes pour un Fluide Incompressible," *Journal of Mécanique*, Vol. 10, No. 3, 1971, p. 357-390.

[7]Kim, J., and Moin, P., "Application of a Fractional-Step Method to Incompressible Navier-Stokes Equations," *Journal of Computational Physics*, Vol. 59, No. 2, 1985, p. 308-323.

[8]Biringen, S., and Danabasoglu, G., "Oscillatory Flow with Heat Transfer in a Square Cavity," *Physics of Fluids A*, Vol. 1, No. 11, 1989, p. 1796-1811.

[9]Biringen, S., Danabosolglu, G., and Eastman, T. K., "A Finite-Difference Method with Direct Solvers for Thermally-Driven Cavity Problems," *Numerical Simulation of Oscillatory Convection in Low-Pr Fluids, Notes on Numerical Fluid Mechanics,* Vol. 27, Viewig, Braunschweig, FRG, 1990, pp. 35-42.